J. Am. Soc. Mass Spectrom. (2019) 30:1964–1972
DOI: 10.1007/s13361-019-02228-0

FOCUS: HONORING HELMUT SCHWARZ'S ELECTION TO THE NATIONAL ACADEMY OF SCIENCES: RESEARCH ARTICLE

Gas-Phase Reactivity of Carbonate Ions with Sulfur Dioxide: an Experimental Study of Clusters Reactions

Anna Troiani, Chiara Salvitti, Giulia de Petris

Dipartimento di Chimica e Tecnologie del Farmaco, "Sapienza" University of Rome, P.le Aldo Moro 5, 00185, Rome, Italy

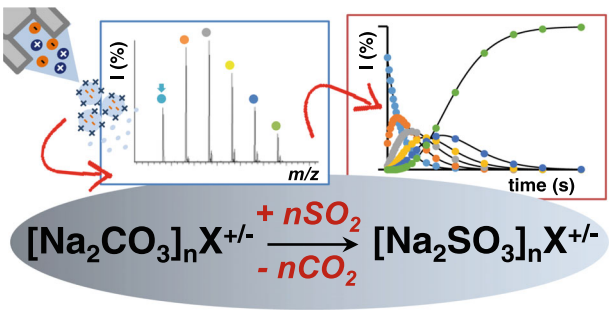

Abstract. The reactivity of carbonate cluster ions with sulfur dioxide has been investigated in the gas phase by mass spectrometric techniques. SO_2 promotes the displacement of carbon dioxide from carbonate clusters through a stepwise mechanism, leading to the quantitative conversion of the carbonate aggregates into the corresponding sulfite cluster ions. The kinetic study of the reactions of positive, negative, singly, and doubly charged ions reveals very fast and efficient processes for all the carbonate ions.

Keywords: Cluster reactivity, Carbonates, Sulfur dioxide, Ion-molecule reactions

Received: 25 February 2019/Revised: 10 April 2019/Accepted: 10 April 2019/Published Online: 8 July 2019

Introduction

Carbonates are among the main reactive components of mineral dust aerosols [1, 2], that play important roles in the radiative balance of Earth [3–5], in cloud condensation and ice nucleation processes [6, 7]. In general, the surface of mineral dust particles as well as that of statues and monuments is a reactive medium for heterogeneous reactions with trace atmospheric gases, thereby altering the atmospheric chemical balance and/or the surface composition. A pollutant mainly emitted from anthropogenic sources is sulfur dioxide [8], also considered one of the most important precursors of atmospheric nucleation particles [9, 10]. SO_2 is transformed into a variety of sulfur compounds by several chemical processes [1, 11–13], that however do not thoroughly explain phenomena such as the explosive growth of sulfate during haze episodes [14]. This has suggested the existence of additional loss mechanisms like, for example, the SO_2 oxidation to sulfate at the interface water—solid phase particles in the troposphere [15–18], the inclusion of which in climate models improves their predictability.

Laboratory studies have long investigated the reaction between carbonates and sulfur dioxide. In particular, the heterogeneous uptake of SO_2 on calcite particles, taken as representative of atmospheric mineral dusts, and the subsequent oxidation by ozone revealed that SO_2 irreversibly binds to the surface as sulfite or bisulfite ion [19]. Also, the reaction commonly known as sulfation of limestone, namely the reaction of solid carbonates with sulfur dioxide, is an old, simple, and economical method used in the abatement of SO_2 emissions from coal combustion activities [20, 21]. Gas-liquid scattering experiments performed with a molten alkali carbonate eutectic have shown that SO_2 is rapidly converted into CO_2 via the reaction SO_2 (g) + CO_3^{2-} → CO_2 (g) + SO_3^{2-} that may occur either at the surface or in a near-surface region [22]. In the gas phase, the reaction of isolated CO_3^- anion with SO_2 to give SO_3^- and CO_2 has been intensively studied [23–26]; it has been found that the rate constant significantly increases upon solvation by 1 to 3 water molecules, in small gaseous clusters.

A convincing modeling of multiphase reactions is indeed provided by gas-phase cluster studies [27–33], that allow

Dedicated to Prof. Dr. Drs. Helmut Schwarz to honor his election to the National Academy of Science

Electronic supplementary material The online version of this article (https://doi.org/10.1007/s13361-019-02228-0) contains supplementary material, which is available to authorized users.

Correspondence to: Anna Troiani; *e-mail:* anna.troiani@uniroma1.it, Giulia Petris; *e-mail:* giulia.depetris@uniroma1.it

insight into fundamental chemical processes without the complications inherent to the bulk or solution. The possibility of varying the size and charge of clusters allows one to investigate the transition from single-molecule to the condensed-phase properties [34]. A paragon of the effectiveness of this microscopic approach to the study of macroscopic phenomena is the major advance obtained in the field of catalysis [35–39].

As a continuation of our interest in the chemistry of sulfur dioxide [40–46] and ionic processes as models of atmospheric reactions [47–50]; here, we report on the gas-phase reactions of SO_2 with positive and negative carbonate cluster ions, investigated by mass spectrometric techniques. Far from being considered nanoparticles, these clusters may be anyhow a model for the sulfation reactions occurring on carbonates or for the reactive uptake of SO_2 in atmospheric mineral aerosols.

Methods

Carbonate cluster ions were generated in the ESI source of a LTQ XL linear ion-trap mass spectrometer (Thermo Fisher Scientific) by spraying millimolar solution of Na_2CO_3 dissolved in water/acetonitrile (1:3). Sample solutions were injected at a flow rate of 5 μL min^{-1} via the onboard syringe pump directly connected to the ESI source. Nitrogen was used as a sheath and auxiliary gas (typical flow rate = 15 and 3 arbitrary units respectively, a.u. ~ 0.37 L min^{-1}). Spray voltage was tuned in the 2–3 kV range to optimize the ion signal with capillary temperature typically fixed at 275 °C. In both polarities, singly and multiply charged species were detected, depending on the voltages applied on the capillary and tube lens. In general, singly charged ions dominate under soft ionization conditions, whereas multiply charged ions are observed by applying mild or harsh voltage potentials.

Ion-molecule reactions were performed on the same mass spectrometer partially modified, as previously described [46]. Briefly, the reagent gas (SO_2) was admitted into the vacuum chamber of the ion trap via a metering valve, and their pressures were measured by a Granville-Phillips Series 370 Stabil Ion Vacuum Gauge after readings calibration [51], also performed by a well-known reaction involving SO_2 as a neutral reagent [25, 26].

After their generation, the ions were thermalized by collisions occurring along the transfer path to the trap. Here, they were in turn isolated with a width of *m/z* 1 and reacted with SO_2. The rate constants were measured by monitoring the signal of the mass-selected reactant ion as a function of the neutral concentration and the time elapsed since the isolation. Typical pressures of SO_2 ranged between 1.0×10^{-7} and 7.2×10^{-7} Torr. For each reaction time, mass spectrum was recorded by setting the normalized collision energy to zero and averaging 10 scan acquisitions. The activation *Q* value was optimized to ensure stable trapping fields for all ions. The water background into the trap was evaluated by using the reactions of Ar^+ ($k = 1.6 \times 10^{-9}$ (± 20%) cm^3 s^{-1} $molecule^{-1}$) as already described [46].

All the reactions can be ascribed to pseudo-first order processes, owing to the excess of neutral gas relative to the reactant ion. This approximation is verified by the logarithmic plots of the reactant species concentration versus time. Experimental data obtained from the kinetics analysis were fitted to a mathematical model consistent with the postulated reaction mechanism by using DynaFit4 software package [52] that performs nonlinear least-squares regression to simultaneously fit reactant and products concentration vs time. To check the validity of the kinetic schemes, the so obtained unimolecular rate constants were used to simulate the time progress of the reactions using the kinetic simulation function contained in DynaFit. The pseudo-first-order rate constants [s^{-1}] thus obtained were divided by the concentration of neutral reagent in the ion trap, deriving the bimolecular rate constants *k* [cm^3 $molecule^{-1}$ s^{-1}]. According to the average dipole orientation (ADO) theory, the reaction efficiency was calculated as the ratio of the bimolecular rate constant *k* to the collision rate constant. To obtain accurate *k* values, approximately 15 independent measurements conducted on different days for each precursor ion were averaged. All rates were measured over a sevenfold neutral pressure range showing linear correlation with the neutral density. The standard deviation in the fitting parameters of the kinetic modeling used is usually evaluated at 10%, whereas the uncertainty attached to the measurement of the neutral pressure is typically evaluated ± 30%.

The MS^n function of LTQ was used to carry out collision-induced dissociation (CID) experiments in the presence of helium as the collision gas (pressure of ca. 3×10^{-3} Torr). The activation time and *Q* values were set to 30 ms and 0.250 respectively, whereas the normalized collision energy was adjusted in the range between 10 and 50% depending on the ion. Full scan mass spectra were recorded in the range of 50–2000 *m/z*. Xcalibur 2.0.6 software was used to acquire all the displayed mass spectra.

Results and Discussion

The ESI (electrospray ionization) spectrum of sodium carbonate solutions is typical of saline solutions in which more salt units (Na_2CO_3) are clustered by positive (Na^+) or negative ($NaCO_3^-$) ions, thereby forming an array of singly and multiply charged cluster ions. In particular, ions having the general formula $[(Na_2CO_3)_n \bullet (Na)_x]^{x+}$ and $[(Na_2CO_3)_n \bullet (NaCO_3)_x]^{x-}$ are observed by positive and negative ESI, respectively, in good agreement with previously obtained results. [53] The source conditions and salt concentration strongly influence the intensities and charge distribution of the observed clusters, and, in general, multiply charged ions are more intense in the negative mode.

Typical mass spectra in the positive and negative ion mode are reported in Figures S1 and S2. In particular, singly charged cluster cations and anions ($x = 1$) are sampled in series having $n = 1$–18 and $n = 0$–18, respectively, in the 50–2000 Da mass range. Doubly charged cluster cations ($x = 2$) are present in

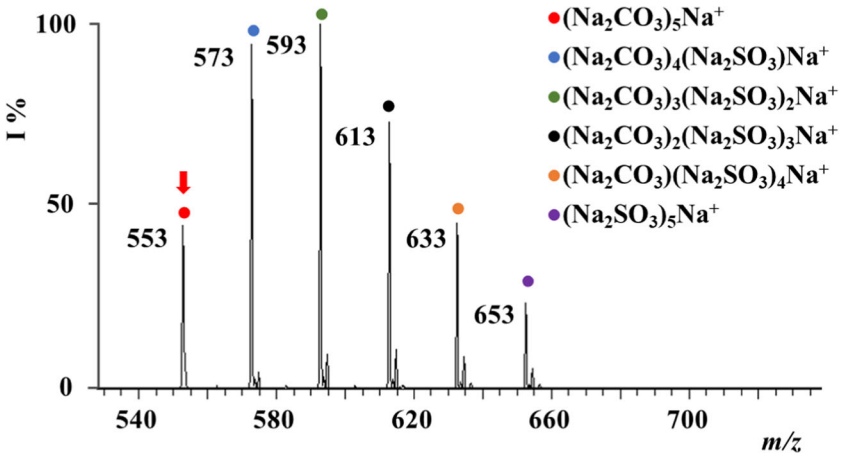

Figure 1. Ion-molecule reaction of isolated $(Na_2CO_3)_5Na^+$ ions (*m/z* 553) with SO_2 at a reaction time of 200 ms. *P* $SO_2 = 2.6 \bullet 10^{-7}$ Torr. The mass-selected precursor ion is denoted by a red arrow

series having $n = 9$–36, whereas the anions have n values that span from 7 to 36. Finally, when $x = 3$, the signals are very small for positive ions ($n = 25$–52), whereas slightly more intense peaks are observed for negative ions with n values ranging from 16 to 54, and when $x = 4$ low signals are observed in the negative mode with $n = 31$–67. Another series observed in both polarities, though intense only for positive ions, shows an additional moiety at *m/z* 40 attributed to NaOH, i.e., $(Na_2CO_3)_n \bullet NaOH \bullet Na^+$ and $[(Na_2CO_3)_n \bullet NaOH \bullet (NaCO_3)]^-$. The formation of OH^- can be reasonably explained taking into account the acid-base properties of carbonate salts that induce the alkalinization of the solution and hence the pH increase of the droplets. Singly charged cluster ions in which the salt units Na_2CO_3 are charged by the CO_3^- or HCO_3^- moieties were not observed.

The gaseous carbonate clusters, either positively or negatively charged, are rather stable species when isolated and submitted to accumulation over long times, in that no signal loss is observed also when exposed to unreactive gas. Conversely, when exposed to SO_2, a significant reactivity is observed. Kinetic studies have been performed under conditions that maximize the intensity of each cluster ion. After mass-selection and reaction with SO_2, all the observed cluster ions—positive, negative, singly and multiply charged ones—show similar characteristics, though with some differences. Accordingly, in the following, the discussion will treat separately the positive and negative species.

Positive Cluster Ions

The positive carbonate cluster ions, isolated in the gas phase, efficiently undergo a sequential reaction with SO_2 that leads to a quantitative conversion of the carbonate

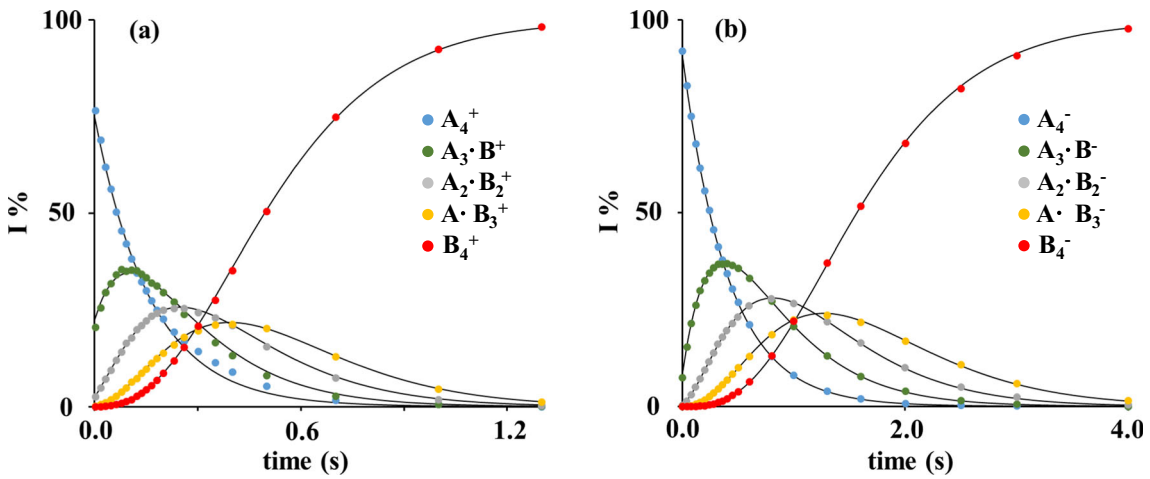

Figure 2. Kinetic plots and best fit lines of the reaction with SO_2 of isolated (**a**) $[(Na_2CO_3)_4Na]^+$ and (**b**) $[(Na_2CO_3)_3NaCO_3]^-$ ions. A = "CO_3" unit; B = "SO_3" unit; Na^+ ions are omitted for the sake of clarity. (**a**) $[(Na_2CO_3)_4Na]^+$ (A_4^+), P $SO_2 = 1.97 \bullet 10^{-7}$ Torr, ● A_4^+ ($R^2 = 0.9972$), ● $A_3 \bullet B^+$ ($R^2 = 0.9971$); ● $A_2 \bullet B_2^+$ ($R^2 = 0.9986$); ● $A \bullet B_3^+$ ($R^2 = 0.9991$); ● B_4^+ ($R^2 = 0.9999$). (**b**) $[(Na_2CO_3)_3NaCO_3]^-$ (A_4^-), P $SO_2 = 0.66 \bullet 10^{-7}$ Torr, ● A_4^- ($R^2 = 0.9998$), ● $A_3 \bullet B^-$ ($R^2 = 0.9999$); ● $A_2 \bullet B_2^-$ ($R^2 = 0.9993$); ● $A \bullet B_3^-$ ($R^2 = 0.9993$); ● B_4^- ($R^2 = 0.9999$)

aggregates into the corresponding sulfite cluster ions. The reaction consists in the stepwise displacement of CO_2 from the carbonate moiety promoted by SO_2, that is concomitantly taken up in the newly formed sulfite cluster, as shown by the following reaction [Eq. (1)].

$$\left[(Na_2CO_3)_n \bullet Na\right]^+ + n\ SO_2 \rightarrow \left[(Na_2SO_3)_n \bullet Na\right]^+ + n\ CO_2 \quad (1)$$

A typical spectrum is reported in Figure 1. The occurrence of sequential displacements of CO_2 by SO_2 has been confirmed by independent experiments in which all the intermediate clusters $[(Na_2CO_3)_{n\text{-}i} \bullet (Na_2SO_3)_i \bullet Na]^+$ (i stands for the step number of the sequence) were in turn isolated after their formation and reacted with SO_2. Reaction 1 is irreversible because no displacement of SO_2 by CO_2 was observed when sulfite clusters were isolated and reacted with variable amount of CO_2, even at the highest pressures and storage times (corresponding to the maximum available time of 10 s).

A kinetic plot showing the time progress of the substitution reactions is reported in Figure 2a for the $[(Na_2CO_3)_4 \bullet Na]^+$ cluster ions, whereas the kinetic plots of all the investigated clusters can be found in Figures S3 and S4. It can be seen that the fully substituted sulfite cluster ions do not undergo any further reactions, with the exception of $[(Na_2SO_3)_2 \bullet (Na)]^+$ (Figure S3a) that adds up to 2 molecules of SO_2, causing the growth of the cluster according to the following reaction [Eq. (2)]:

$$\left[(Na_2SO_3)_2 \bullet (Na)\right]^+ + m\ SO_2 \rightarrow \left[(Na_2SO_3)_2 \bullet (SO_2)_m \bullet (Na)\right]^+ \ (m = 1, 2) \quad (2)$$

After the first SO_2 addition, a competition between the addition of a second molecule of SO_2 and one of H_2O is observed, with the last one being faster. Interestingly, the addition products were not observed neither on the initial carbonate clusters nor on the partially substituted ones. On the contrary, the carbonate clusters containing a NaOH moiety, i.e., $[(Na_2CO_3)_n \bullet NaOH \bullet (Na)]^+$ ($n = 2$–11) give a minor channel corresponding to the SO_2 addition.

$$[(Na_2CO_3)_n \bullet NaOH \bullet (Na)]^+ + SO_2 \rightarrow [(Na_2CO_3)_{n-1} \bullet (Na_2SO_3) \bullet (NaOH) \bullet (Na)]^+ + CO_2 \quad (3a)$$

$$[(Na_2CO_3)_n \bullet (NaOH) \bullet (SO_2) \bullet (Na)]^+ \quad (3b)$$

The results of the kinetic study of the CO_2–SO_2 exchange and SO_2 (H_2O) addition reactions are illustrated in Table 1. Due to the superimposition of doubly charged ions on singly charged ones, that becomes increasingly important in $(Na_2CO_3)_nNa^+$ cluster ions with $n \geq 7$, it was possible to measure the rate constants only for clusters with $n = 1$–6. Table 1 reports, for each singly charged cluster ion, the measured bimolecular rate constants k_i (cm^3 $molecule^{-1}$ s^{-1}) of each CO_2 displacement that has been modeled with the following consecutive scheme.

$$\left[(Na_2CO_3)_n \cdot Na\right]^+ + SO_2 \xrightarrow{k_1} \left[(Na_2CO_3)_{n-1} \cdot (Na_2SO_3) \cdot Na\right]^+ + CO_2 \quad (4)$$

$$\left[(Na_2CO_3)_{n-1} \bullet Na_2SO_3 \bullet Na\right]^+ SO_2 \xrightarrow{k_2} \left[(Na_2CO_3)_{n-2} \bullet (Na_2SO_3)_2 \bullet Na\right]^+ + CO_2 \quad (5)$$

$$\left[(Na_2CO_3)_{n-2} \bullet (Na_2SO_3)_2 \bullet Na\right]^+ + (n-2)\ SO_2 \xrightarrow{k_3 \rightarrow k_{i=n}} \left[(Na_2SO_3)_n \bullet Na\right]^+ + (n-2)\ CO_2 \quad (6)$$

As shown, the smallest cluster ion with $n = 1$ is the least reactive one; its only CO_2 moiety is exchanged at the rate constant k_1 equal to 1.64×10^{-12} cm^3 $molecule^{-1}$ s^{-1}, corresponding to ca. 1.4 reactive collision in 1000. This is not unexpected because, based on its computed D_{3h} structure [54], the direct interaction of

Table 1. Rate Constants[§] and Efficiencies[#] of the SO_2–CO_2 Exchange Reactions of Selected $(Na_2CO_3)_n \bullet Na^+$ and $(Na_2CO_3)_n \bullet NaOH \bullet Na^+$. Rate Constants[§] and Efficiencies[#] of the SO_2 (H_2O) Addition Reaction of Selected $(Na_2SO_3)_n \bullet Na^+$, $(Na_2CO_3)_n \bullet NaOH \bullet Na^+$ and $(Na_2SO_3)_n \bullet NaOH \bullet Na^+$ Cluster Ions. $k \times 10^{-9}$ cm^3 $molecule^{-1}$ s^{-1} (Efficiency %)

SO_2–CO_2 exchange	k_1	k_2	k_3	k_4	k_5	k_6
$Na_2CO_3 \bullet Na^+$	0.00164 (0.14)					
$(Na_2CO_3)_2 \bullet Na^+$	0.924 (85)	1.20 (111)				
$(Na_2CO_3)_3 \bullet Na^+$	0.904 (90)	1.08 (103)	1.11 (105)			
$(Na_2CO_3)_4 \bullet Na^+$	0.916 (89)	1.09 (106)	1.09 (106)	1.08 (105)		
$(Na_2CO_3)_5 \bullet Na^+$	0.992 (97)	1.10 (108)	1.11 (109)	1.08 (106)	0.830 (82)	
$(Na_2CO_3)_6 \bullet Na^+$	0.990 (98)	0.940 (93)	0.722 (72)	0.940 (93)	0.719 (71)	0.125 (12)
$(Na_2CO_3)_2 \bullet NaOH \bullet Na^+$	0.632 (59)	0.875 (82)				
$(Na_2CO_3)_3 \bullet NaOH \bullet Na^+$	0.711 (68)	0.628 (60)	0.664 (64)			
$(Na_2CO_3)_4 \bullet NaOH \bullet Na^+$	0.699 (68)	0.615 (60)	0.582 (57)	0.645 (63)		
SO_2 (H_2O) addition	$k_{1a(SO2)}$	$k_{b(2SO2)}$	$k_{c(H2O)}$			
$(Na_2SO_3)_2 \bullet Na^+$	0.0239 (2.2)	0.0501 (4.8)	0.486 (28)			
$(Na_2CO_3)_2 \bullet NaOH \bullet Na^+$	0.00481 (0.5)					
$(Na_2CO_3)_3 \bullet NaOH \bullet Na^+$	0.0117 (1.1)					
$(Na_2CO_3)_4 \bullet NaOH \bullet Na^+$	0.00780 (0.8)					
$(Na_2SO_3)_2 \bullet NaOH \bullet Na^+$	5.99 (56)	0.213 (2.0)				
$(Na_2SO_3)_3 \bullet NaOH \bullet Na^+$	5.42 (52)					
$(Na_2SO_3)_4 \bullet NaOH \bullet Na^+$	6.71 (66)					

[§]± 30% (see text); [#]efficiency = k_n/k_{ADO}

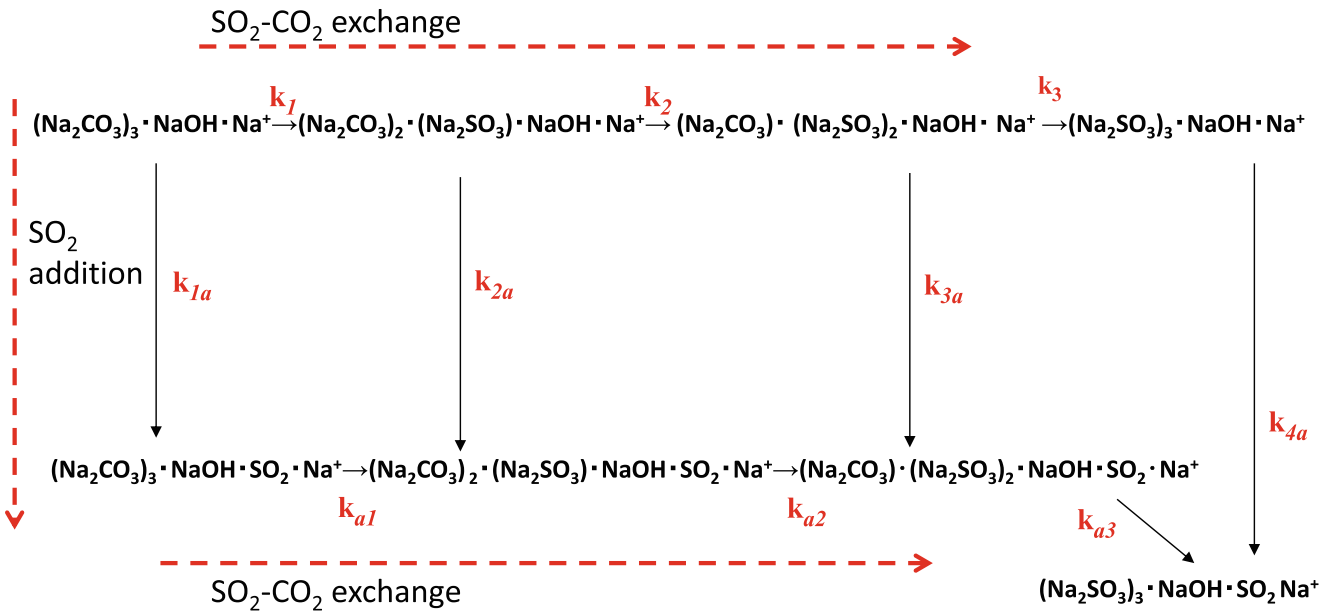

Scheme 1. Schematic of the SO_2–CO_2 exchange and SO_2 addition reactions observed by reaction of $[(Na_2CO_3)_3•NaOH•Na]^+$ ions with SO_2

the three sodium cations with the oxygen atoms hampers and slows the reaction with SO_2. Conversely, all the other clusters show very fast and efficient substitution reactions.

A common and interesting feature is that, within a specific cluster, the substitution rate and efficiency slightly enhance passing from the first to the second step, remaining comparable in the subsequent steps. In larger clusters ($n = 5$–6), the rate constant decreases in the last step ($[(Na_2CO_3)_5Na]^+$) and already after the first substitution ($k_2 < k_1$) in the highest cluster investigated ($[(Na_2CO_3)_6Na]^+$).

A rationale for this behavior is that the higher polarizability of sulfite clusters with respect to that of carbonate clusters facilitates the approach and the uptake of SO_2, making the successive substitution faster. However, in large and partially substituted clusters, the probability of reactive collisions of the incoming SO_2 with a carbonate unit may be reduced by the steric hindrance and structural problems.

As anticipated, the presence of a NaOH molecule within the carbonate cluster changes the reactivity. For comparison purposes, Table 1 also reports the rate constants of the reactions observed in carbonate cluster cations containing NaOH ($n = 2$–4). The salient differences are (1) the slower SO_2-CO_2 exchange compared with the clusters not containing NaOH, (2) the minor channel corresponding to the SO_2 addition (see Eq. (3b)), (3) the higher rate and efficiency of the SO_2 addition to fully substituted sulfite cluster ions. The kinetic scheme is however more complicated than illustrated in reactions (3a) and (3b). As an example of the observed reactivity, the whole process and the time profile of $[(Na_2CO_3)_3•(NaOH)•(Na)]^+$ are reported in Scheme 1 and Figure S5. As outlined in Scheme 1, the products of the SO_2–CO_2 exchange (3a) in turn continue both the SO_2 exchange and SO_2 addition, the products of the addition reaction (3b) in turn undergo the SO_2–CO_2 exchange. The measured rate constants for the assayed clusters with $n = 2$–3 are reported in Table 2.

Although the intensity of higher cluster ions $[(Na_2CO_3)_n•(NaOH)•(Na)]^+$ ($n > 3$) did not allow a kinetic study, an interesting reactivity can be observed by isolation of the $[(Na_2CO_3)_n•(NaOH)•(SO_2)•(Na)]^+$ addition products ($n > 3$) which carry out both an intermolecular (7a) and an intracluster (7b) SO_2–CO_2 exchange. As an example, a rough estimate of the (7a)/(7b) ratio in the $[(Na_2CO_3)_4•(NaOH)•(SO_2)•(Na)]^+$ cluster ion amounts to ca. 10/1.

Table 2. Rate Constants[§] and Efficiencies[#] of the Reactions Summarized in Scheme 1. k*na* Refer to the SO_2 Addition Reactions of the $(Na_2CO_3)_n•NaOH•Na^+$ Ions and their SO_2 Exchange Products (see Scheme 1). k*an* Refer to the SO_2-CO_2 Exchange Reactions of the SO_2 Addition Products. $k \times 10^{-10}$ cm^3 $molecule^{-1}$ s^{-1} (Efficiency %)

	SO_2 addition			
Cluster ion	k*1a*	k*2a*	k*3a*	k*4a*
$(Na_2CO_3)_2•NaOH•Na^+$	0.0481 (0.5)	0.123 (1.1)	6.07 (57)	
$(Na_2CO_3)_3•NaOH•Na^+$	0.117 (1.1)	0.099 (0.9)	0.872 (8.4)	5.42 (52)
	SO_2–CO_2 exchange			
Cluster ion	k*a1*	k*a2*	k*a3*	
$(Na_2CO_3)_2•NaOH•SO_2•Na^+$	1.45 (14)	5.06 (48)		
$(Na_2CO_3)_3•NaOH•SO_2•Na^+$	3.85 (37)	4.41 (52)	0.416 (4.0)	

[§]± 30% (see text); [#]efficiency = k_n/k_{ADO}

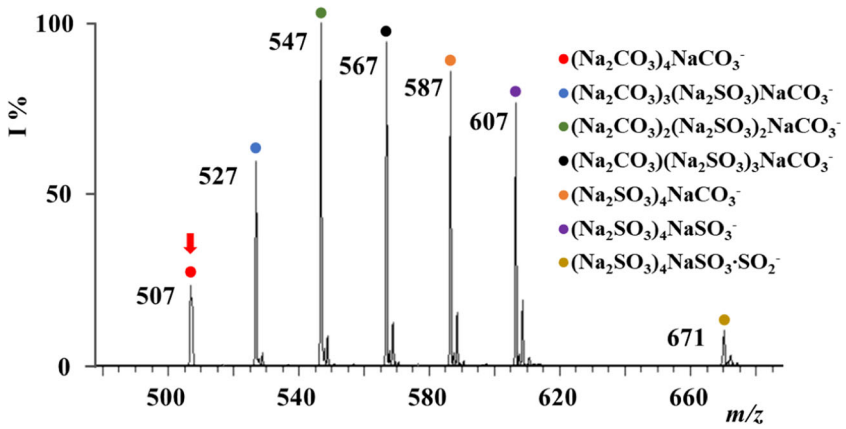

Figure 3. Ion-molecule reaction of isolated $(Na_2CO_3)_4NaCO_3^-$ ions (*m/z* 507) with SO_2 at a reaction time of 300 ms. *P* $SO_2 = 2.6 \cdot 10^{-7}$ Torr. The mass-selected precursor ion is denoted by a red arrow

$$[(Na_2CO_3)_n \bullet (NaOH) \bullet (SO_2) \bullet (Na)]^+ \xrightarrow{+\,SO_2} \begin{cases} \xrightarrow{-\,CO_2} [(Na_2CO_3)_{n-1} \bullet (Na_2SO_3) \bullet (NaOH) \bullet (SO_2) \bullet (Na)]^+ & (7a) \\ \xrightarrow{-\,CO_2} [(Na_2CO_3)_{n-1} \bullet (Na_2SO_3) \bullet (NaOH) \bullet (Na)]^+ & (7b) \end{cases}$$

Accordingly, a different reactivity can be envisaged in the assayed cluster ions. The carbonate clusters and partially SO_2 substituted ones undergo the SO_2–CO_2 exchange reaction without generally forming SO_2 addition products, which points to a direct reaction between the carbonate ion and SO_2 once the latter adds to the cluster. The presence of NaOH makes the reaction slower and little amounts of SO_2 addition products are detectable, though they are significantly depleted by the efficient subsequent SO_2–CO_2 exchange reaction (Table 2). In higher clusters ($n > 3$), likely conformational effects allow both the intracluster and intermolecular reaction with the captured and external SO_2, respectively (Figures S6 and S7).

Negative Cluster Ions

Similar to the cluster cations, the carbonate cluster anions $[(Na_2CO_3)_n \bullet (NaCO_3)]^-$ very efficiently undergo the quantitative conversion into the corresponding sulfite cluster ions. In these cluster ions, the charge is given by the $NaCO_3^-$ group that is also an exchangeable group upon exposure to SO_2. Consequently, both the charged $NaCO_3^-$ and the neutral Na_2CO_3 groups can be susceptible of reaction, and are thus treated as equivalent towards the reaction with sulfur dioxide [Eq. (8)]. A typical spectrum is reported in Figure 3.

$$\left[(Na_2CO_3)_n \bullet (NaCO_3)\right]^- + (n+1)\,SO_2 \rightarrow \left[(Na_2SO_3)_n \bullet (NaSO_3)\right]^- + (n+1)\,CO_2 \quad (8)$$

Like for positive ions, the sequential nature of the process has been confirmed by isolation and reaction with SO_2 of the intermediate clusters $[(Na_2CO_3)_{n-i} \bullet (Na_2SO_3)_i \bullet NaCO_3]^-$. Likewise, the addition of SO_2 only occurs to fully substituted sulfites; however, different from the cluster cations, it is observed with all the anions but $[(Na_2CO_3)_3 \bullet (NaCO_3)]^-$ (Table 3).

$$\left[(Na_2SO_3)_n \bullet (NaSO_3)\right]^- + m\,SO_2 \rightarrow \left[(Na_2SO_3)_n \bullet (SO_2)_m \bullet (NaSO_3)\right]^- \quad (m = 1, 2) \quad (9)$$

The kinetic plot of Figure 2b reports the time profile of the observed reactions for the $[(Na_2CO_3)_3 \bullet (NaCO_3)]^-$ ions, whereas the kinetic plots of all the investigated clusters can

Table 3. Rate Constants[§] and Efficiencies[#] of the SO_2-CO_2 Exchange and SO_2 Addition Reactions of Selected $(Na_2CO_3)_n \bullet NaCO_3^-$ and $(Na_2SO_3)_n \bullet NaSO_3^-$ Cluster Ions, $k \times 10^{-9}$ cm^3 $molecule^{-1}$ s^{-1} (Efficiency %)

SO_2–CO_2 exchange	k_1	k_2	k_3	k_4	k_5
$NaCO_3^-$	1.29 (100)				
$Na_2CO_3 \bullet NaCO_3^-$	1.13 (101)	1.01 (92)			
$(Na_2CO_3)_2 \bullet NaCO_3^-$	1.07 (100)	1.06 (100)	1.02 (96)		
$(Na_2CO_3)_3 \bullet NaCO_3^-$	1.04 (100)	1.01 (98)	0.976 (94)	0.903 (88)	
$(Na_2CO_3)_4 \bullet NaCO_3^-$	1.03 (100)	1.00 (98)	0.988 (97)	0.957 (94)	0.885 (87)
SO_2 addition	$k_{1a(SO2)}$	$k_{b(2SO2)}$			
$NaSO_3^-$	0.424 (35)				
$Na_2SO_3 \bullet NaSO_3^-$	0.0452 (4.1)				
$(Na_2SO_3)_2 \bullet NaSO_3^-$	0.103 (10)	0.0467 (4.5)			
$(Na_2SO_3)_4 \bullet NaSO_3^-$	0.205 (20)	0.0066 (0.66)			

[§]± 30% (see text); [#]efficiency = k_n/k_{ADO}

Table 4. Rate Constants[§] and Efficiencies[#] of the SO_2–CO_2 Exchange of Selected $(Na_2CO_3)_nNa_2^{2+}$ and $(Na_2CO_3)_n(NaCO_3)_2^{2-}$ Cluster Ions. Rate Constants[§] and Efficiencies[#] of the SO_2 Addition Reactions of $(Na_2SO_3)_n(NaSO_3)_2^{2-}$ Cluster Ions. $k \times 10^{-9}$ cm^3 $molecule^{-1}$ s^{-1} (Efficiency %)

	k_1	k_2	k_3	k_4	k_5	k_6	k_7	k_8	k_9	k_{10}	k_{11}	k_{12}	k_{13}
SO_2–CO_2 exchange													
$(Na_2CO_3)_9 \bullet Na_2^{2+}$	1.04 (101)	1.12 (109)	1.31 (128)	1.19 (116)	1.02 (100)	0.933 (91)	1.02 (100)	0.839 (82)	1.09 (107)	1.04 (101)			
$(Na_2CO_3)_{13} \bullet Na_2^{2+}$	1.24 (123)	0.979 (97)	0.502 (50)	0.151 (15)	0.286 (28)	0.643 (64)	0.864 (86)	0.506 (50)	0.380 (38)	1.27 (126)	0.859 (86)	0.406 (40)	0.031 (3.0)
$(Na_2CO_3)_9 \bullet (NaCO_3)_2^{2-}$	1.10 (108)	1.10 (108)	1.07 (105)	1.09 (108)	1.06 (104)	1.07 (105)	1.03 (102)	1.01 (100)	0.984 (97)	0.926 (91)	0.417 (41)	1.10 (108)	
$(Na_2CO_3)_{11} \bullet (NaCO_3)_2^{2-}$	1.12 (111)	1.07 (105)	1.08 (107)	1.10 (109)	1.07 (106)	1.09 (108)	1.07 (106)	1.13 (112)	1.03 (102)	1.02 (101)	0.998 (99)	0.997 (99)	0.280 (28)
SO_2 addition	$k_{1a(SO2)}$	$k_{b(2SO2)}$											
$(Na_2SO_3)_9 \bullet (NaSO_3)_2^{2-}$	0.244 (24)	0.291 (29)											
$(Na_2SO_3)_{11} \bullet (NaSO_3)_2^{2-}$	0.455 (45)	0.113 (11)											

[§]± 30% (see text); [#]efficiency = k_n/k_{ADO}

be found in Figures S8 and S9. Table 3 reports the bimolecular rate constants k_i (cm^3 $molecule^{-1}$ s^{-1}) of the CO_2-SO_2 exchange of $[(Na_2CO_3)_n \bullet (NaCO_3)]^-$ ions and the SO_2 addition reactions of $[(Na_2SO_3)_n \bullet (NaSO_3)]^-$ ions. They were measured for singly charged cluster anions with $n = 0–4$, that have $n+1$ exchangeable units (i.e., $[(Na_2CO_3)_4NaCO_3]^-$ has five exchangeable CO_2 units). The subsequent adducts with $n > 4$ show a superimposition with the doubly charged ions and were not sampled. The CO_2–SO_2 exchange was modeled according to the following scheme:

$$\left[(Na_2CO_3)_n \bullet NaCO_3\right]^- + SO_2 \xrightarrow{k_1} \left[(Na_2CO_3)_{n-1} \bullet Na_2SO_3 \bullet NaCO_3\right]^- + CO_2 \quad (10)$$

$$\left[(Na_2CO_3)_{n-1} \bullet Na_2SO_3 \bullet NaCO_3\right]^- + SO_2 \xrightarrow{k_2} \left[(Na_2CO_3)_{n-2} \bullet (Na_2SO_3)_2 \bullet NaCO_3\right]^- + CO_2 \quad (11)$$

$$\left[(Na_2CO_3)_{n-2} \bullet (Na_2SO_3)_2 \bullet NaCO_3\right]^- + (n-1)\ SO_2 \xrightarrow{k_3 \rightarrow k_{i=n+1}} \left[(Na_2SO_3)_{(n)} \bullet NaSO_3\right]^- + (n-1)\ CO_2 \quad (12)$$

The kinetic results show that the exchange reactions are very fast and occur at the collision rate for all the negatively charged carbonate clusters. As the size of the cluster increases, a slight decrease of the rate constants is observed starting from k_3. Finally, as observed for positive ions, the addition of SO_2 to the sulfite anions occurs with rate constants lower than those measured for the displacement reactions.

Doubly Charged Cluster Ions

For both positive and negative doubly charged ions, it was possible to follow the exchange reactions and to measure the relative rate constants only for a few clusters. An example is given in Figure S10. In particular, only those having an odd n value do not overlap with the singly charged peaks. Further to this, due to the fact that large clusters have unresolved and spread signals of too low intensities, the series is restricted to $n = 9$, 13 and $n = 9$, 11 for positive and negative ions, respectively (Table 4). Lastly, for the same reason, no kinetic analysis was possible for the triply charged species, therefore hampering a more systematic analysis on the behavior of multiply charged species. Despite the low number of clusters studied, it is evident that a common feature of both positive and negative ions is the high rate constants of all the displacement steps that often exceed the collision rate (Figure S11), with the exception of $[(Na_2CO_3)_{13}(Na)_2]^{2+}$ that displays a clear irregular trend. The addition of SO_2 is observed only with the negative clusters $[(Na_2CO_3)_9(NaCO_3)_2]^{2-}$ and $[(Na_2CO_3)_{11}(NaCO_3)_2]^2$

$^{-}$, that reversibly add two sulfur dioxide molecules. Nonetheless, the number of clusters sampled is unfortunately very limited which does not allow a systematic study.

Conclusions

In the gas phase carbonate cluster ions, positive or negative, singly and doubly charged, are efficiently converted into the corresponding sulfite ions by reaction with SO_2. The reaction occurs through a stepwise displacement of CO_2. The kinetic study has shown that the charge plays a major role in the smallest clusters, $Na_3CO_3^+$ and $NaCO_3^-$, which makes the former far less reactive than the latter. Conversely, the higher clusters have similar kinetic features, pointing to a minor effect of the charge that is spread over the larger aggregates. Clusters containing a NaOH molecule show a different reactivity consisting in the addition of SO_2 and in the competition between an intracluster and intermolecular SO_2/CO_2 exchange. In addition, structural effect can be responsible for the decrease or the irregularity of the reaction rate observed, for example, in the doubly charged cluster ions.

Acknowledgements

The financial support by "Sapienza" University of Rome is gratefully acknowledged. The authors thank Stefania Recaldin for helpful assistance.

References

1. Seinfeld, J.H., Pandis, S.N.: Atmospheric chemistry and physics: from air pollution to climate change, 3th edn. John Wiley and Sons, Inc., New York (2016)
2. Dentener, F.J., Carmichael, G.R., Zhang, Y., Lelieveld, J., Crutzen, P.J.: Role of mineral aerosol as a reactive surface in the global troposphere. J. Geophys. Res.-Atmos. **101**, 22869–22889 (1996)
3. Bellouin, N., Boucher, O., Haywood, J., Reddy, M.S.: Global estimate of aerosol direct radiative forcing from satellite measurements. Nature. **438**, 1138–1141 (2005)
4. Yu, H., Kaufman, Y.J., Chin, M., Feingold, G., Remer, L.A., Anderson, T.L., Balkanski, Y., Bellouin, N., Boucher, O., Christopher, S., DeCola, P., Kahn, R., Koch, D., Loeb, N., Reddy, M.S., Schulz, M., Takemura, T., Zhou, M.: A review of measurement-based assessments of the aerosol direct radiative effect and forcing. Atmos. Chem. Phys. **6**, 613–666 (2006)
5. Scanza, R.A., Mahowald, N., Ghan, S., Zender, C.S., Kok, J.F., Liu, X., Zhang, Y., Albani, S.: Modeling dust as component minerals in the community atmosphere model: development of framework and impact on radiative forcing. Atmos. Chem. Phys. **15**, 537–561 (2015)
6. Lohmann, U., Feichter, J.: Global indirect aerosol effects: a review. Atmos. Chem. Phys. **5**, 715–737 (2005)
7. DeMott, P.J., Sassen, K., Poellot, M.R., Baumgardner, D., Rogers, D.C., Brooks, S.D., Prenni, A.J., Kreidenweis, S.M.: African dust aerosols as atmospheric ice nuclei. Geophys. Res. Lett. **30**, 1732–1735 (2003)
8. Stern, D.I.: Global sulfur emissions from 1850 to 2000. Chemosphere. **58**, 163–175 (2005)
9. Duparta, Y., Kinga, S.M., Nekat, B., Nowak, A., Wiedensohler, A., Herrmann, H., David, G., Thomas, B., Miffre, A., Rairoux, P., D'Anna, B., George, C.: Mineral dust photochemistry indices nucleation events in the presence of SO_2. Proc. Natl. Acad. Sci. **109**, 20842–20847 (2012)
10. Curtius, J.: Nucleation of atmospheric aerosol particles. C. R. Phys. **7**, 1027–1045 (2006)
11. Rattigan, O.V., Boniface, J., Swartz, E., Davidovits, P., Jayne, J.T., Kolb, C.E., Worsnop, D.R.: Uptake of gas-phase SO_2 in aqueous sulfuric acid: oxidation by H_2O_2, O_3 and HONO. J. Geophys. Res.-Atmos. **105**, 65–78 (2000)
12. Zuo, Y., Hoigne, J.: Evidence for photochemical formation of H_2O_2 and oxidation of SO_2 in authentic fog water. Science. **260**, 71–73 (1993)
13. Chandler, A.S., Choularton, T.W., Dollard, G.J., Eggleton, A.E.J., Gay, M.J., Hill, T.A., Jones, B.M.R., Tyler, B.J., Bandy, B.J., Penkett, S.A.: Measurements of H_2O_2 and SO_2 in clouds and estimates of their reaction rate. Nature. **336**, 562–565 (1988)
14. Wang, Y., Zhang, Q., Jiang, J., Zhou, W., Wang, B., He, K., Duan, F., Zhang, Q., Philip, S., Xie, Y.: Enhanced sulfate formation during China's severe winter haze episode in January 2013 missing from current models. J. Geophys. Res.-Atmos. **119**(17), 10425–10440 (2014)
15. Zheng, B., Zhang, Q., Zhang, Y., He, K.B., Wang, K., Zheng, G.J., Duan, F.K., Ma, Y.L., Kimoto, T.: Heterogeneous chemistry: a mechanism missing in current models to explain secondary inorganic aerosol formation during the January 2013 haze episode in North China. Atmos. Chem. Phys. **15**, 2031–2049 (2015)
16. Ullerstam, M., Vogt, R., Langer, S., Ljungstr¨om, E.: The kinetics and mechanism of SO_2 oxidation by O_3 on mineral dust. Phys. Chem. Chem. Phys. **4**, 4694–4699 (2002)
17. Laskin, A., Gaspar, D.J., Wang, W., Hunt, S.W., Cowin, J.P., Colson, S.D., Finlayson-Pitts, B.J.: Reactions at interfaces as a source of sulfate formation in sea-salt particles. Science. **301**, 340–344 (2003)
18. Hung, H.M., Hoffmann, M.R.: Oxidation of gas-phase SO_2 on the surfaces of acidic microdroplets: implications for sulfate and sulfate radical anion formation in the atmospheric liquid phase. Environ. Sci. Technol. **49**, 13768–13776 (2015)
19. Usher, C.R., Al-Hosney, H., Carlos-Cuellar, S., Grassian, V.H.: A laboratory study of the heterogeneous uptake and oxidation of sulfur dioxide on mineral dust particles. J. Geophys. Res. **107**, 4713–4721 (2002)
20. Hu, G., Dam-Johansen, K., Wedel, S., Hansen, J.P.: Review of the direct sulfation reaction of limestone. Prog. Energy Combust. Sci. **32**, 386–407 (2006)
21. McIlroy, R.A., Atwood, G.A., Major, C.J.: Absorption of sulfur dioxide by molten carbonates. Environ. Sci. Technol. **7**, 1022–1028 (1973)
22. Krebs, T., Nathanson, G.M.: Reactive collisions of sulfur dioxide with molten carbonates. Proc. Natl. Acad. Sci. **107**, 6622–6627 (2010)
23. Fehsenfeld, F.C., Schmeltekopf, A.L., Schiff, H.I., Ferguson, E.E.: Laboratory measurements of negative ion reactions of atmospheric interest. Planet. Space Sci. **15**, 373–379 (1967)
24. Albritton, D.L., Dotan, I., Streit, G.E., Fahey, D.W., Fehsenfeld, F.C., Ferguson, E.E.: Energy dependence of the O^- transfer reactions of O_3^- and CO_3^- with NO and SO_2. J. Chem. Phys. **78**, 6614–6619 (1983)
25. Seeley, J.V., Morris, R.A., Viggiano, A.A.: Rate constants for the reactions of $CO_3^-(H_2O)_{n=0-5} + SO_2$: implications for CIMS detection of SO_2 detection. Geophys. Res. Lett. **24**, 1379–1382 (1997)
26. Miller, T.M., Friedman, J.F., Williamson, J.S., Viggiano, A.A.: Rate constants for the reactions of CO_3^- and O_3^- with SO_2 from 300 to 1440 K. J. Chem. Phys. **124**, 144305–144305 (2006)
27. Castleman Jr., A.W.: Cluster structure and reactions: gaining insights into catalytic processes. Catal. Lett. **141**, 1243–1253 (2011)
28. Ertl, G.: Reactions at surfaces: from atoms to complexity. Angew. Chem. Int. Ed. **47**, 3524–3535 (2008)
29. Schlangen, M., Schwarz, H.: Effects of ligands, cluster size, and charge state in gas-phase catalysis: a happy marriage of experimental and computational studies. Catal. Lett. **142**, 1265–1278 (2012)
30. Schwarz, H.: How and why do cluster size, charge state, and ligands affect the course of metal-mediated gas-phase activation of methane? Isr. J. Chem. **54**, 1413–1431 (2014)
31. Feyel, S., Schroder, D., Schwarz, H.: Pronounced cluster-size effects: gas-phase reactivity of bare vanadium cluster cations Y_n^+ (n = 1-7) toward methanol. J. Phys. Chem. A. **113**, 5625–5632 (2009)
32. Schlangen, M., Schwarz, H.: Probing elementary steps of nickel-mediated bond activation in gas-phase reactions: ligand- and cluster-size effects. J. Catal. **284**, 126–137 (2011)
33. Zhang, X., Schwarz, H.: Generation of gas-phase nanosized vanadium oxide clusters from a mononuclear precursor by solution nucleation and electrospray ionization. Chem. Eur. J. **16**, 1163–1167 (2010)
34. Castleman, A.W.j., Keesee, R.G.: Gas-phase clusters: spanning the states of matter. Science. **241**, 36–42 (1988)

35. Böhme, D.K., Schwarz, H.: Gas-phase catalysis by atomic and cluster metal ions: the ultimate single-site catalysts. Angew. Chem. Int. Ed. **44**, 2336–2354 (2005)
36. Schröder, D., Schwarz, H.: Gas-phase activation of methane by ligated transition-metal cations. Proc. Natl. Acad. Sci. **105**, 18114–18119 (2008)
37. Li, J., Zhou, S., Zhang, J., Schlangen, M., Usharani, D., Shaik, S., Schwarz, H.: Mechanistic variants in gas-phase metal-oxide mediated activation of methane at ambient conditions. J. Am. Chem. Soc. **138**, 11368–11377 (2016)
38. Schwarz, H.: Ménage-à-trois: single-atom catalysis, mass spectrometry, and computational chemistry. Cat. Sci. Technol. **7**, 4302–4314 (2017)
39. Geng, C., Li, J., Weiske, T., Schwarz, H.: Ta_2^+-mediated ammonia synthesis from N_2 and H_2 at ambient temperature. Proc. Natl. Acad. Sci. **115**, 11680–11687 (2018)
40. Troiani, A., Rosi, M., Garzoli, S., Salvitti, C., de Petris, G.: Effective redox reactions by chromium oxide anions: sulfur dioxide oxidation in the gas phase. Int. J. Mass Spectrom. **436**, 18–22 (2019)
41. Troiani, A., Rosi, M., Garzoli, S., Salvitti, C., de Petris, G.: Vanadium hydroxide cluster ions in the gas phase: bond-forming reactions of doubly-charged negative ions by SO_2 promoted V−O activation. Chem. Eur. J. **23**, 11752–11756 (2017)
42. Troiani, A., Rosi, M., Garzoli, S., Salvitti, C., de Petris, G.: Sulphur dioxide cooperation in hydrolysis reactions of vanadium oxide and hydroxide cluster dianions. New J. Chem. **42**, 4008–4016 (2018)
43. de Petris, G., Troiani, A., Rosi, M., Angelini, G., Ursini, O.: Methane activation by metal-free radical cations: experimental insight into the reaction intermediate. Chem. Eur. J. **15**, 4248–4252 (2009)
44. de Petris, G., Cartani, A., Troiani, A., Angelini, G., Ursini, O.: Water activation by SO_2^+ ions: an effective source of OH radicals. Phys. Chem. Chem. Phys. **11**, 9976–9978 (2009)
45. de Petris, G., Cartani, A., Rosi, M., Barone, V., Puzzarini, C., Troiani, A.: The proton affinity and gas-phase basicity of sulfur dioxide. ChemPhysChem. **17**, 112–115 (2011)
46. de Petris, G., Cartani, A., Troiani, A., Barone, V., Cimino, P., Angelini, G., Ursini, O.: Double C-H activation of ethane by metal-free $SO_2^{\cdot+}$ radical cations. Chem. Eur. J. **16**, 6234–6242 (2010)
47. Troiani, A., Rosi, M., Salvitti, C., de Petris, G.: The oxidation of sulfur dioxide by single and double oxygen transfer paths. ChemPhysChem. **15**, 2723–2731 (2014)
48. Cacace, F., Cipollini, R., de Petris, G., Rosi, M., Troiani, A.: A new sulfur oxide, OSOSO, and its cation, likely present in the Io's atmosphere: detection and characterization by mass spectrometric and theoretical methods. J. Am. Chem. Soc. **123**, 478–484 (2001)
49. Cacace, F., de Petris, G., Pepi, F., Rosi, M., Troiani, A.: Ionization of ozone/chlorofluorocarbon mixtures in atmospheric gases: formation and remarkable dissociation of $[CHXYO_3]^+$ complexes (X = H, Cl, F; Y= Cl, F). Chem. Eur. J. **6**, 2572–2581 (2000)
50. Cacace, F., de Petris, G., Pepi, F., Troiani, A.: Direct experimental evidence for the $H_2O^+O_2^-$ charge transfer complex: crucial support to atmospheric photonucleation theory. Angew. Chem. Int. Ed. **39**, 367–369 (2000)
51. Bartmess, J.E., Georgiadis, R.M.: Empirical methods for determination of ionization gauge relative sensitivities for different gases. Vacuum. **33**, 149 (1983)
52. Kuzmic, P.: Program DYNAFIT for the analysis of enzyme kinetic data: application to HIV proteinase. Anal. Biochem. **237**, 260–273 (1996)
53. Hao, C., March, R.E.: Electrospray ionization tandem mass spectrometric study of salt cluster ions: part 2- salts of polyatomic acid groups and of multivalent metals. J. Mass Spectrom. **36**, 509–521 (2001)
54. Dean, P.A.W.: The not-so-simple coordination chemistry of alkali-metal cations Li^+, Na^+ and K^+ with one carbonate anion: a study using density functional and atoms in molecules theories. Inorg. Chim. Acta. **469**, 245–254 (2018)